ChemSusChem

Research Article
doi.org/10.1002/cssc.202202241

Chemistry Europe
European Chemical Societies Publishing

www.chemsuschem.org

SiCO Ceramics as Storage Materials for Alkali Metals/Ions: Insights on Structure Moieties from Solid-State NMR and DFT Calculations

Edina Šić,[a] Jochen Rohrer,*[b] Emmanuel III Ricohermoso,[c] Karsten Albe,[b] Emmanuel Ionescu,[c, d] Ralf Riedel,[c] Hergen Breitzke,[a] Torsten Gutmann,*[a] and Gerd Buntkowsky*[a]

Polymer-derived silicon oxycarbide ceramics (SiCO) have been considered as potential anode materials for lithium- and sodium-ion batteries. To understand their electrochemical storage behavior, detailed insights into structural sites present in SiCO are required. In this work, the study of local structures in SiCO ceramics containing different amounts of carbon is presented. ^{13}C and ^{29}Si solid-state MAS NMR spectroscopy combined with DFT calculations, atomistic modeling, and EPR investigations, suggest significant changes in the local structures of SiCO ceramics even by small changes in the material composition. The provided findings on SiCO structures will contribute to the research field of polymer-derived ceramics, especially to understand electrochemical storage processes of alkali metal/ions such as Na/Na^+ inside such networks in the future.

Introduction

Electrochemical energy storage has been at the forefront of strategies for sustainable energy systems taking significant leaps in development in the past decades. Much attention has been drawn to lithium batteries due to their high energy density which is considered a major requirement in energy storage systems.[1] The steadily growing global market necessitates the development of novel material technologies that can provide both improved physicochemical properties for efficient energy storage and cover environmental and economic aspects. In this context, a variety of novel materials with tailored properties have been explored for use as electrodes in batteries, replacing the commercially utilized graphite.[2,3] Silicon-based polymer-derived ceramics (PDCs) including silicon oxycarbide (SiCO) or silicon carbonitride (SiCN) have been proven as efficient electrode materials for rechargeable lithium batteries,[2,4,5] and very recently for Na/Na^+ cell model systems as the basis for sodium batteries.[6,7] The amorphous covalent framework of SiCO/SiCN, where Si atoms are coordinated to O as well as to C or N and where domains of disordered free carbon nanosheets are assumed, enables reversible lithium storage with improved charge capacity compared to conventional graphite electrodes. Hereby, the PDCs do not undergo large volume expansion and thus supply better cycling performance than the analogous graphite materials,[8,9] making them excellent candidates as electrodes for all-solid-state batteries. Additionally, PDCs are also used as catalyst supports,[10,11] semiconductors,[12] sensing elements,[13] drug delivery systems[14] as well as for high-temperature[15] and electromagnetic applications.[16] These applications became feasible due to the specific physicochemical properties of PDCs such as outstanding mechanical strength,[8] high chemical[10] and thermal stability,[17,18] corrosion and oxidation resistance[18,19] as well as their low density and high porosity.[20]

Rosenburg et al.[21] correlated the ordering and the content of sp^2 carbon domains in SiCO to its charge transport mechanism by analyzing samples with 0 to approximately 58 vol% carbon contents. Aside from the carbon content, the thermal treatment,[5,15,36–44] and shaping conditions (spinning, foaming, warm pressing, extrusion, printing, etc.),[10,22,23,24] affect the chemical architecture of the ceramic. Silicon oxycarbide (SiCO) follows a corner-sharing tetrahedral structure of SiC_xO_{4-x} ($x = 0$–4)[25] and can be described as a glassy network of vitreous silica glasses, with carbon partly replacing oxygen. Multiple studies using various characterization techniques including IR

[a] E. Šić, Dr. H. Breitzke, Dr. T. Gutmann, Prof. G. Buntkowsky
Eduard Zintl Institute for Inorganic and Physical Chemistry
Technical University of Darmstadt, 64287 Darmstadt (Germany)
E-mail: gutmann@chemie.tu-darmstadt.de
gerd.buntkowsky@chemie.tu-darmstadt.de
[b] Dr. J. Rohrer, Prof. K. Albe
Department of Materials and Earth Sciences, Materials Modelling Division
Technical University of Darmstadt, 64287 Darmstadt (Germany)
E-mail: rohrer@mm.tu-darmstadt.de
[c] Dr. E. I. Ricohermoso, Dr. E. Ionescu, Prof. R. Riedel
Department of Materials and Earth Sciences, Group of Dispersive Solids
Technical University of Darmstadt, 64287 Darmstadt (Germany)
[d] Dr. E. Ionescu
Fraunhofer IWKS, Department of Digitalization of Resources
Brentanostr. 2a, 63755 Alzenau (Germany)

Supporting information for this article is available on the WWW under https://doi.org/10.1002/cssc.202202241

This publication is part of a joint Special Collection of ChemSusChem, Batteries & Supercaps, and Energy Technology including invited contributions focusing on the "International Conference on Sodium Batteries (ICNaB)". Please visit chemsuschem.org/collections to view all contributions.

© 2023 The Authors. ChemSusChem published by Wiley-VCH GmbH. This is an open access article under the terms of the Creative Commons Attribution Non-Commercial NoDerivs License, which permits use and distribution in any medium, provided the original work is properly cited, the use is non-commercial and no modifications or adaptations are made.

© 2023 The Authors. ChemSusChem published by Wiley-VCH GmbH

spectroscopy, Raman spectroscopy, XRD, small-angle X-ray scattering (SAXS), NMR analysis, TGA/MS, and TEM have been conducted to validate the structural transformation of SiCO at different thermal treatment stages.[10,21,23–27]

Despite being a valuable alternative electrode material in energy storage systems,[19,28] the structural role and the quantity of the formed phases in PDCs have shown complexity and require further investigations for deeper understanding.[29,30] Therefore, a more systematic evaluation of the PDC structure at the nanoscale as a function of manufacturing parameters (i.e. precursor composition, temperature) is necessary to successfully optimize processing routes and performance of PDC systems.

In this study, we report the impact of various commercially available polymeric precursors on the nanostructure of synthesized SiCOs. Within the final SiCO network, the amount of incorporated carbon and the phase distribution of the formed species should be controlled by the composition of the polysiloxane precursor (i.e., by modification of the alkyl side chain to vinyl or/and phenyl groups in the polymeric precursor), as well as by the temperature where the thermal cross-linking reaction is performed.

Insight into the local chemical environment of the various SiC_xO_{4-x} tetrahedral units and sp^2-bonded carbon phases in the prepared SiCOs is provided by applying ^{29}Si MAS NMR as well as $^1H\rightarrow^{29}Si$ and $^1H\rightarrow^{13}C$ CPMAS NMR. The interpretation of the NMR spectroscopic data is supported by quantum chemical calculations at the DFT level of theory. For these calculations, model systems are created that realistically represent the chemical composition of the materials.

This improved structural characterization of SiCOs combining experimental data from solid-state NMR with quantum chemical calculations and modeling will contribute significantly to the development of novel materials for sustainable energy storage, especially for advancement in the battery field.[6,31]

Experimental Methods

Material synthesis

The synthesis of PDCs with varying carbon content is already published in detail in Refs.[21,32] Typically, SiCO-C14% (MK-PMS), SiCO-C24% (SPR-212), SiCO-C36% (SILRES-604), and SiCO-C55% (RD-684) were prepared from commercially available polymethylsilsesquioxane (Belsil PMS MK and Silres 604, Wacker GmbH, Burghausen, Germany), and polysiloxanes (SPR-212 and SPR 684, Starfire Systems Inc., NY, USA), respectively. These polymers were cross-linked in an alumina tube furnace at 250 °C for two hours under flowing argon atmosphere. Subsequently, the cross-linked samples were heated at 1100 °C for three hours. The heating and cooling rates were 100 K h^{-1}. The obtained glassy chunks were crushed and sieved to a grain size of <40 μm. The elemental composition of each synthesized sample is given in the Supporting Information (Table S1).

Solid-state NMR spectroscopy

The preceramic polymers (MK-PMS, SPR-212, SILRES-604, and RD-684) and the SiCO-PDCs after thermal cross-linking were studied by applying ^{29}Si and ^{13}C solid-state NMR (ssNMR). Measurements were carried out on a Bruker Avance III HD NMR spectrometer at a magnetic field of 7 T corresponding to frequencies of 59.62 MHz for ^{29}Si and 75.47 MHz for ^{13}C. Hereby, a 4 mm double resonance probe was used allowing spinning of the samples at 10 kHz. All chemical shifts are given with respect to tetramethylsilane (TMS = 0 ppm). ^{29}Si spectra were referenced using kaolinite (−92.5 ppm) as an external standard. ^{13}C chemical shifts were referenced using glycine as an external standard employing the signal of the C=O group (176.5 ppm).

For recording of ^{29}Si MAS NMR spectra of the preceramic polymers MK-PMS and SILRES-604 as well as of all four SiCO-PDCs the Hahn-echo sequence was applied using 90° and 180° pulses of 5 μs and 10 μs, respectively. The pulse spacing τ was set to two rotor periods and a repetition time of 40 s was adopted collecting 2000 scans for each ^{29}Si MAS NMR spectrum. The liquid preceramic precursors SPR-212 and RD-684 were investigated by performing single-pulse ^{29}Si NMR experiments under static conditions collecting 355 scans using a single pulse sequence. Again a 90° pulse of 5 μs and a repetition time of 40 s were utilized in these experiments.

^{13}C MAS NMR spectra of the SiCO-PDCs were recorded with the Hahn-echo sequence employing a 90° excitation pulse of 3 μs and refocusing the magnetization by a 180° pulse of 6 μs. One rotor period and a repetition delay of 40 s were chosen. Each spectrum was recorded with 4320 scans except the ^{13}C MAS NMR spectrum of the SiCO-C14% sample, which was recorded with 10720 scans. The ^{13}C NMR spectra of the liquid preceramic precursors SPR-212 and RD-684 were measured under static conditions collecting 355 scans using a single pulse sequence. Again a 90° pulse of 3 μs and a repetition delay of 40 s were utilized in these experiments.

$^1H\rightarrow^{29}Si$ CPMAS NMR and $^1H\rightarrow^{13}C$ CPMAS NMR experiments were performed using the ramped CPMAS sequence with a linear 50–100 ramp on the ^1H channel. For the polarization transfer between ^1H and ^{29}Si nuclei, a contact time of 7.5 ms was employed, whereas a contact time of 2 ms was used in $^1H\rightarrow^{13}C$ CPMAS NMR experiments. $^1H\rightarrow^{29}Si$ CPMAS spectra were recorded with a recycle delay of 8 s, and $^1H\rightarrow^{13}C$ CPMAS NMR spectra using a recycle delay of 5 s. To obtain $^1H\rightarrow^{29}Si$ CPMAS and $^1H\rightarrow^{13}C$ CPMAS spectra of the PDC materials 15000 scans were collected. 3333 scans were used to accumulate the $^1H\rightarrow^{13}C$ CPMAS NMR spectra of the starting materials MK-PMS and SILRES-604. Due to the high conductivity of several of the samples, no decoupling was applied during data acquisition.

Deconvolutions of the line shapes of the 1D solid-state NMR spectra were performed with the Origin Pro software using Gaussian/Lorentzian lines. The parameters obtained from the deconvolution are listed in Tables S2, S4, S6, and S8, respectively.

For sample SiCO-C14%, a frequency-switched Lee–Goldburg heteronuclear correlation (FSLG HETCOR) experiment was measured on a Bruker Avance III HD NMR spectrometer at 14.1 T corresponding to a frequency of 150.92 MHz for ^{13}C and 600.12 for ^1H. Using a 3.2 mm rotor the sample was spun at 10 kHz. A 90° excitation pulse of 2.5 μs was applied to the ^1H channel. During the evolution of the ^1H chemical shift, homonuclear ^1H decoupling was applied with a B_1 field strength of 100 kHz. Cross polarization (CP) transfer was then performed employing a linear ramp on the ^1H channel during a contact time of 0.5 ms to ensure the observation of short-range correlations. During data acquisition, heteronuclear ^1H decoupling with the tppm15 sequence was applied.[33] A repetition delay of 4 s was used and 2048 scans were accumulated for each of the 32 slides yielding a measuring time of about 3 days. The ^{13}C chemical shift was referenced to TMS. To reference the indirect ^1H dimension, an additional ^1H-^1H MAS FSLG spectrum was recorded according to ref. [34]. The ^1H direct dimension in this spectrum was referenced

© 2023 The Authors. ChemSusChem published by Wiley-VCH GmbH

to TMS using adamantane (1.78 ppm) as external standard, whereas the indirect ^{1}H dimension was referenced by selecting one diagonal peak from the ^{1}H-^{1}H MAS FSLG spectrum. The ^{1}H indirect dimension of the ^{1}H-^{13}C FSLG-HETCOR MAS NMR spectrum was adjusted according to this reference

EPR spectroscopy

EPR data were collected on an EPR Miniscope MS-400 (Magnettech, Germany) equipped with an ATC H03 temperature controller and a rectangular TE102 resonator operating at 9.43 GHz. The room temperature EPR spectra were recorded sweeping the magnetic field in a range of 5.97 mT with a center B_0 field of 337 mT. All EPR spectra were collected as single scans of 120 s sweeping time with 4096 points of digital resolution. The microwave attenuation was 40 dB and the modulation amplitude was set to 0.2 mT.

Atomistic modeling

Supplementing the experimental measurements, we performed density functional theory (DFT) calculations[35–40] to predict theoretical chemical shifts of silicon and carbon in amorphous SiCO. In particular, we focused on the variation of such shifts originating from a variety of different local chemical environments. The considered local environments are depicted in Figure 1a. For silicon, we studied ideal 4-fold coordination with O and C neighbors, represented by SiO_4 (pure local silica), SiC_1O_3, SiC_2O_2, SiC_3O and SiC_4 (pure local silicon carbide) structure motifs; for carbon we considered CC_3 (pure local graphite / graphene), CSi_4 (pure local silicon carbide) and CH_2Si_2 structure motifs (hydrogen saturated carbon on an O site in silica). In contrast to previous atomistic models[41–45] that were dealing with full 3D representation of SiCO, we here used an ideally coordinated silica network to embed the various local building blocks (Figure 1b) and constructed an amorphous carbon network (Figure 1c) containing 72% 3-fold-, 23% 4-fold-, and 5% 2-fold-coordinated C. These pure models were obtained by molecular-dynamics cook-and-quench simulations[46] using classical[47] and machine-learned[48] interatomic potentials followed by full structure optimizations based on density functional theory relaxations.[35,36]

Relaxed structures were subjected to further DFT calculation as to simulate chemical shifts.[37–39] As reference for these shifts, we used tetramethylsilane (TMS, $Si(CH_3)_4$). For further details concerning the embedding of C in SiO_2 and computational parameters, see the Supporting Information

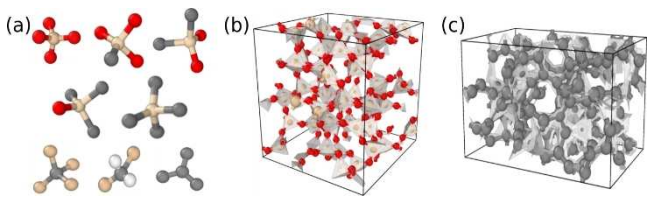

Figure 1. Local chemical environments for Si and C (a) and atomistic models for SiO_2 (b) and disordered carbon (c). Color coding: Si: tan; C: gray; O: red; H: white.

Results and Discussion

Simulated NMR chemical shifts

The distributions of calculated NMR shifts for the different local chemical environments are shown in Figure 2. For Si we obtain -103 ± 11 ppm (SiO_4, 1070 local environments), -70 ± 15 ppm (SiC_1O_3, 161 local environments), -39 ± 10 ppm (SiC_2O_2, 320 local environments), -10 ± 10 ppm (SiC_4, 6 local environments) and -3 ± 16 ppm (SiC_3O, 9 local environments). For ^{13}C, we obtain 80 ± 18 ppm (CSi_4, 47 structures) and 153 ± 18 ppm (CC_3, 98 structures) for ideally coordinated atoms; for C replacing O in a silica network, we obtain a shift of 16 ± 2 ppm (CSi_2H_2, 8 structures). These results will be discussed in the following in the context of experimental spectra.

^{29}Si solid-state NMR spectroscopy

The ^{29}Si MAS NMR spectra of the siloxane polymer precursors, as well as the Hahn-echo ^{29}Si MAS and $^{1}H \rightarrow {}^{29}Si$ CPMAS NMR spectra of the PDCs containing different carbon content together with the line shape analysis and signal assignment are shown in Figure 3. Details on the line shape analysis for each spectrum are given in Tables S1–S4. By comparing the signal widths in the ^{29}Si MAS NMR spectra of the PDCs (Figure 3b) with the ^{29}Si MAS NMR spectra of their corresponding precursor polymers (PMS-MK, SPR-212, SILRES-604, and RD-684; Figure 3a)

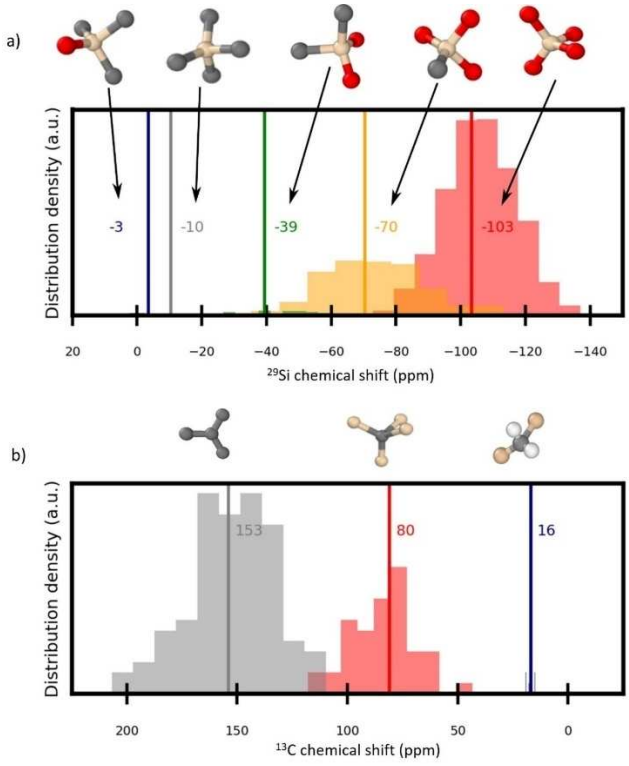

Figure 2. Simulated NMR chemical shifts for (a) Si and (b) C with various local bonding environments relative to TMS.

© 2023 The Authors. ChemSusChem published by Wiley-VCH GmbH

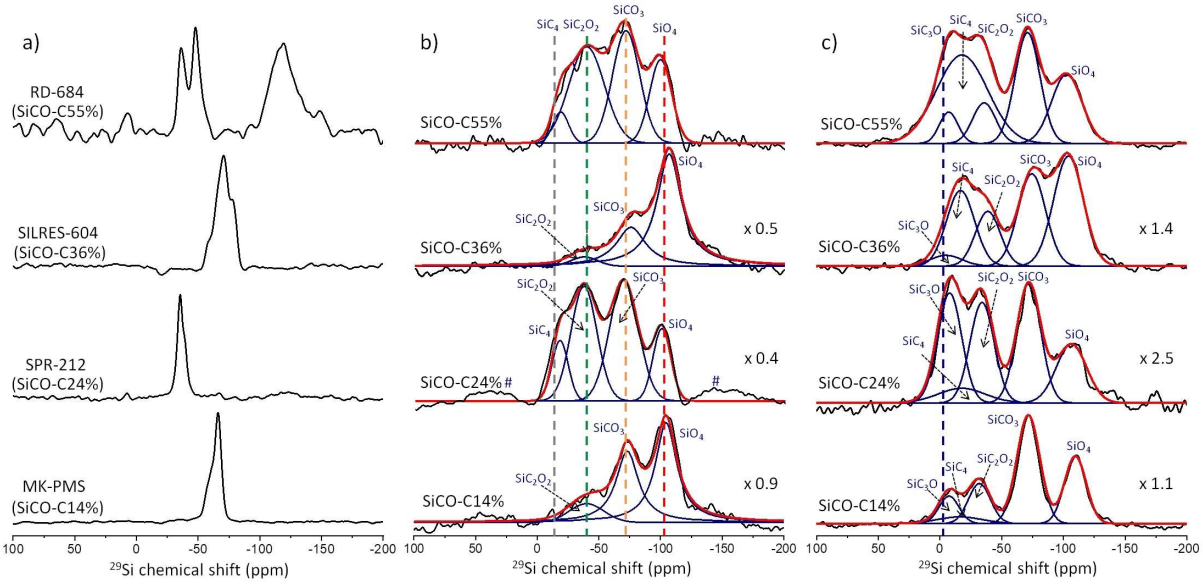

Figure 3. a) Hahn-echo ^{29}Si MAS NMR spectra of the preceramic precursors PMS-MK and Silres-604, and static ^{29}Si NMR spectra of SPR-212 and SPR-684 obtained with single pulse excitation. b) Hahn-echo ^{29}Si MAS NMR spectra and c) ^{1}H→^{29}Si CPMAS NMR spectra of the SiCO-PDCs with various carbon content between 14–55 %. Note: All spectra were recorded at 7 T. Black solid lines show the experimental ^{29}Si NMR spectra of the PDCs, the deconvolutions are represented by blue lines, and cumulative curves are shown in red. Vertical dashed lines indicate averaged calculated chemical shifts for various local environments. # denotes imperfect phase correction. The detailed overview of the line shape analysis is provided in Tables S2–S5. MAS spectra were recorded at 10 kHz spinning.

significant changes are detected. Whereas the precursors exhibit very narrow signal widths between 425 Hz and 1355 Hz, a significant broadening to widths between 1700 and 5600 Hz is obtained for the PDCs. These changes are attributed to an increase in local structural disorder leading to a broader distribution of isotropic chemical shifts in the PDCs.[49] Moreover, also the ranges of isotropic chemical shifts have changed significantly. Whereas the ^{29}Si NMR spectra of the precursor polymers MK-PMS and SILRES-604 contain isotropic signals in the region between −50 and −75 ppm, the SPR-212 and RD-684 preceramics yield resonances between −25 and −60 ppm. Additionally, the ^{29}Si MAS NMR spectrum of RD-684 contains a broad signal in the region between −100 and −160 ppm attributed to impurities. This signal probably originates from siloxane groups known as Q^4 and Q^3 sites present in the synthetic process of RD-684.[50]

In contrast to the precursor materials, the Hahn-echo ^{29}Si MAS NMR spectra of the C-rich PDCs contain isotropic chemical shifts distributed along the whole spectral region between 0 and −150 ppm arising from different environments of SiC_xO_{4-x} sites. These spectral changes clearly indicate cross-linking of the four precursor materials into the PDC network with high disordered structure.

The Hahn-echo ^{29}Si MAS NMR spectra (Figure 3b) of the C-rich PDCs can be deconvoluted into four combined Gaussian–Lorentzian lines. The results of the deconvolution [isotropic shifts (δ) and signal widths (fwhm)] are collected in Tables S2 and S3. Hereby, attention should be paid to a challenging deconvolution analysis due to the signal broadening and overlapping signals caused by the presence of dipole-dipole interactions, anisotropic interaction, and paramagnetic species. From the deconvolution a tentative peak assignment based on the literature[4,25,27,30,45,51,52] is performed. The averaged isotropic chemical shifts at −102, −72, −38, and −17 ppm are assigned to SiC_4, SiC_2O_2, $SiCO_3$, and SiO_4 structural units present in the PDC network.

Comparing the ^{1}H→^{29}Si CPMAS NMR spectra (Figure 3c) with the Hahn-echo ^{29}Si MAS NMR spectra (Figure 3b) of the PDCs, significant changes in the signal line shapes are noticed. The ^{1}H→^{29}Si CPMAS NMR spectra of the PDCs show a wider spectral range up to around 180 ppm compared to the Hahn echo ^{29}Si MAS NMR spectra. ^{1}H→^{29}Si CPMAS NMR spectra are deconvoluted with five Gaussian/Lorentzian lines. The parameters isotropic chemical shift (δ) and line widths (fwhm) of the deconvolutions are listed in ESI in Table S4–S5. The obtained chemical shifts are attributed to SiO_4 (ca. −104 ppm), $SiCO_3$ (ca. −73 ppm), SiC_2O_2 (ca. −40 ppm) and SiC_4 (ca. −16 ppm), respectively. In addition, a new signal at around −7 ppm has appeared in the ^{1}H→^{29}Si CPMAS NMR spectra, which is attributed to SiC_3O moieties[25,51] containing protons in their close vicinity which are most probably located close to the surface. The locations of these five peaks are in good agreement with our theoretical calculations as indicated by the dashed vertical lines in Figure 3c, thus verifying association of the various peaks with the respective local chemical environments. Compared to the Hahn-echo ^{29}Si MAS NMR, the signal intensities in ^{1}H→^{29}Si CPMAS NMR show significant differences, and there are apparent small shifts of the resonances. Such differences are well-known from silica materials (for example, see ref. [53]) and caused by the cross-polarization (CP) from

© 2023 The Authors. ChemSusChem published by Wiley-VCH GmbH

$^{1}H \rightarrow {}^{29}Si$. The CP selectively detects the signal of silicon nuclei in the close vicinity of a hydrogen atom. Thus, signals of silicon nuclei in sites without neighboring hydrogen nuclei are strongly suppressed or invisible in $^{1}H \rightarrow {}^{29}Si$ CPMAS NMR spectra.

^{13}C solid-state NMR spectroscopy

The ^{13}C MAS NMR spectra of the silicon-based PDCs including the NMR studies of their precursor polymers are shown in Figure 4. The ^{13}C NMR spectra of the precursor materials (MK-PMS, SPR-212, SILRES-604, and RD-684; Figure 4a) all consist of a narrow signal between −2 and −6 ppm. This signal is assigned to sp^3 organic moieties such as CH_3 and CH_2 groups bonded to silicon atoms.[54–56] Furthermore, signals in the chemical shift range between 100 and 150 ppm are obtained, which are typical for carbon atoms in functionalized vinyl and aromatic side chains.[55,56] In contrast, in the Hahn-echo ^{13}C MAS NMR spectra of the PDCs after thermal cross-linking (Figure 4b), significantly wider isotropic chemical shift ranges of −50 and 200 ppm are covered. This observation is similar to the findings obtained in the ^{29}Si ssNMR studies (Figure 3) and again clearly suggests cross-linking of the used preceramic polymers into the PDC with the increased structural disorder.

Comparing the Hahn-echo ^{13}C MAS NMR spectra of the four PDCs, a significant signal intensity increase with growing carbon content in the network is obtained. This improvement of the signal-noise ratio in the Hahn-echo ^{13}C MAS NMR spectra most probably refers to the increased formation of free carbon phases in the PDC network when carbon-richer polymer precursors are cross-linked.

Each Hahn-echo ^{13}C MAS NMR spectrum of the PDCs (Figure 4b) was deconvoluted by several Gaussian/Lorentzian lines. The parameters isotropic shifts (δ) and signal widths (fwhm) used in these deconvolutions are given in Tables S6 and S7. In all Hahn-echo ^{13}C MAS NMR spectra of the ceramics, a large spread of the chemical shifts within the range of 50 to 200 ppm is noticed. This indicates various local environments of sp^2-bonded carbon atoms in the structure. In addition, the Hahn-echo ^{13}C MAS NMR spectra of SiCO-C14% and SiCO-C24% exhibit an isotropic signal at approximately 24 ppm originating from sp^3 hybridized C.[57] This signal does not appear in the Hahn-echo spectra of materials with higher carbon content such as SiCO-C55% and SiCO-C36%. Such observation is most probably related to the limited formation of sp^3 carbon species when carbon-rich precursor polymers are used in the manufacturing process of PDCs.

The $^{1}H \rightarrow {}^{13}C$ CPMAS NMR spectra (Figure 4c) exhibit better resolution than the Hahn-echo ^{13}C CPMAS NMR (Figure 4b). The parameters δ and fwhm used for the deconvolution of the $^{1}H \rightarrow {}^{13}C$ CPMAS NMR spectra are given in Tables S8 and S9. The overlapping resonances at 15 and −13 ppm are assigned to sp^3 bonded carbon species such as CSi_4 and SiC_xO_{4-x}, and probably remaining aliphatic carbons from the manufacturing process, whereas the signals at 135 ppm originate from sp^2 carbon according to the literature.[25,51,54] Note, that the shift of the signal at −13 ppm in the $^{1}H \rightarrow {}^{13}C$ CPMAS NMR to higher field compared to ref.[51] is caused by its overlapping with the spinning side bands. Interestingly, an additional signal at around 175 ppm is obtained in each $^{1}H \rightarrow {}^{13}C$ CPMAS NMR. Deeper analysis of this signal by $^{1}H \rightarrow {}^{13}C$ CPMAS NMR experiments at different spinning rates (for SiCO-C14% sample shown

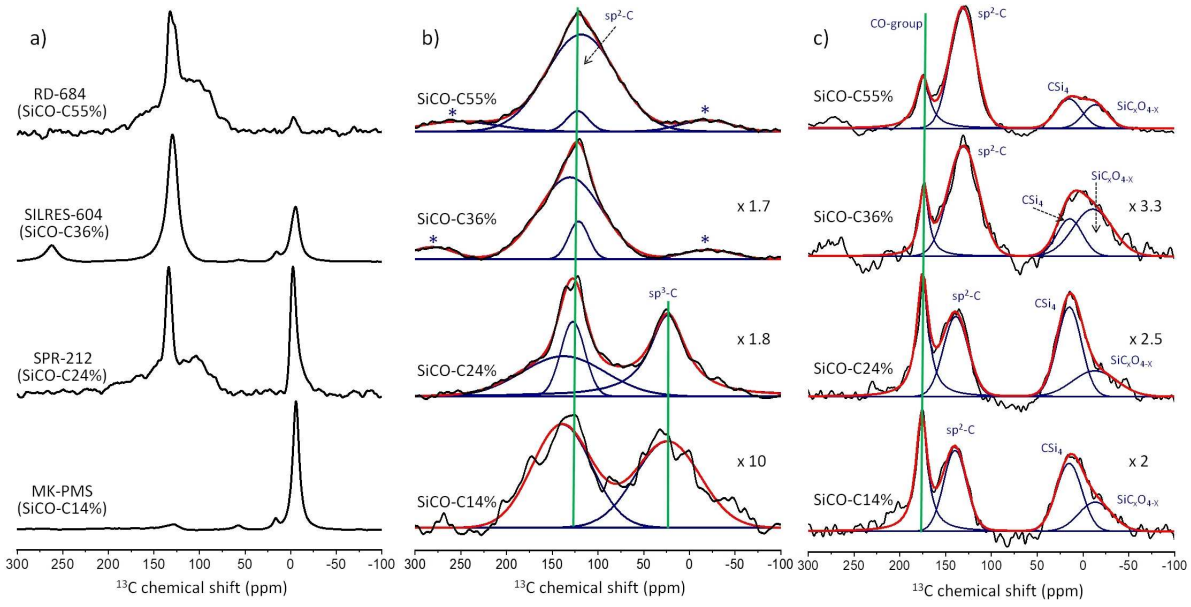

Figure 4. a) $^{1}H \rightarrow {}^{13}C$ CPMAS NMR spectra of the preceramic precursors MK-PMS and SILRES-604 at 10 kHz and static ^{13}C NMR spectra obtained with single pulse excitation of SPR-212 and RD-684. b) Hahn-echo ^{13}C MAS NMR spectra of PDCs SiCO-C14%, SiCO-C24%, SiCO-C36%, and SiCO-C55%. c) $^{1}H \rightarrow {}^{13}C$ CPMAS NMR spectra of the PDCs with various carbon amounts. Note: All spectra were recorded at 7 T. The experimental ^{13}C NMR spectra are shown by black lines, the deconvoluted spectra by blue lines, and cumulative curves are shown in red. MAS spectra were recorded at 10 kHz spinning. The chemical shifts are listed in Tables S6 – S9. The green lines are to guide the eyes.

© 2023 The Authors. ChemSusChem published by Wiley-VCH GmbH

in Figure S1) shows that this signal does not refer to a spinning side band as proposed in the literature.[25,57] Moreover, the isotropic signal at 175 ppm indicates the presence of carbonyl containing sites (C=O-group) such as carbonates.[58] This signal is not clearly visible in the Hahn-echo ^{13}C MAS NMR spectra, probably due to signal broadening or slow relaxation of C=O carbons.

To resolve the carbon–hydrogen environment in the SiCO network, a ^{1}H-^{13}C FSLG-HETCOR MAS NMR spectrum of SiCO-C14% as a model system was recorded. The spectrum achieved at 14.1 T after 3 days of measurement is shown in Figure 5. Applying this experiment, different sp^3 hybridized carbon resonances with similar ^{13}C NMR chemical shifts in the range between 25 and 50 ppm are resolved clearly. These resonances show strong correlations to hydrogens at 2.6 and 8.7 ppm in the ^{1}H indirect dimension. Furthermore, the signal at 175 ppm assigned to C=O containing sites also correlates to these protons. Finally, a signal at around 15 ppm is visible which correlates with hydrogens at 1 ppm in the indirect dimension. Such correlation signal most probably originates from remaining aliphatic carbons from the manufacturing process. This is in good agreement with the results from $^{1}H\rightarrow^{13}C$ CPMAS NMR spectroscopy (Figure 4c), where a clear assignment of the aliphatic carbon species was not feasible since signals in the aliphatic region are overlapping with CSi_4 and SiC_xO_{4-x} resonances.

The protons at 2.6 ppm, which are in the typical range of aliphatic protons, seem to be surrounded by sp^3 carbon species, whereas the strong deshielded protons at 8.7 ppm indicate the presence of paramagnetic centers in their local environment. Most probably, the protons at 8.7 pm originate from defects in aggregated carbon phases.

In contrast, the signal at around 135 ppm attributed to the sp^2 bonded carbon obtained in the $^{1}H\rightarrow^{13}C$ CPMAS NMR spectrum at 7 T (Figure 4c, sample SiCO-C14%) is not visible in the ^{1}H-^{13}C FSLG-HETCOR MAS NMR at 14.1 T. Furthermore, the signal at 135 ppm is also not visible in the $^{1}H\rightarrow^{13}C$ CPMAS NMR spectrum recorded at 14.1 (Figure S2). A plausible explanation for this observation is the strong effect of paramagnetism which influences the relaxation time of the protons. As a result of the large electronic magnetic moment, a rapid nuclear relaxation is induced diminishing the efficient magnetic polarization transfer on the sp^2 bonded carbon spins at 14.1 T. The impact of the unpaired electrons on the enhanced nuclear relaxation results in reduced signal intensity or signal blending into the baseline at the higher magnetic field. For a deeper discussion of this effect, the reader is referred to refs.[59]

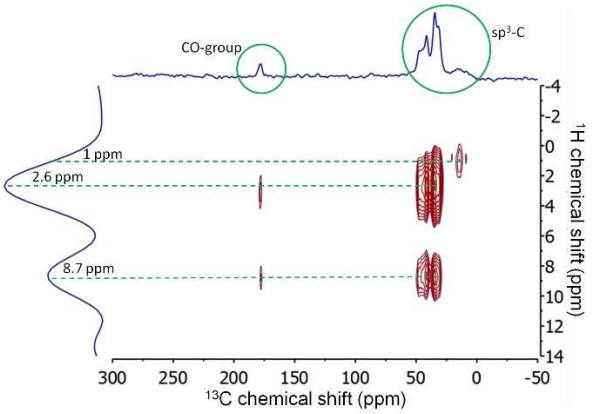

Figure 5. The ^{1}H-^{13}C FSLG-HETCOR MAS NMR spectrum of SiCO-C14% recorded at 14.1 T shows the correlation between the ^{13}C resonances of the sp^3 carbon species and C=O containing sites with the ^{1}H resonances at 2.6 ppm, 8.7 ppm, and 1 ppm. Note: The spectrum was recorded at 14.1 T.

A comparison of experimental to calculated ^{13}C chemical shifts shows considerably less good agreement as compared to the ^{29}Si chemical shifts. In addition to an overall drift of calculated peak positions towards higher shifts, the peak separation between sp^3-like C and CSi_4 is underestimated by ~20 ppm. Yet here we emphasize that CH_2Si_2 structure units (H-saturated C on an O site in amorphous silica) are expected to result in a sharp peak at $\sim -60 \pm 2$ ppm relative to the CSi_4 signal. However, no sharp peak to the right of the CSi_4 signal is observed in the experimental spectra. This points towards the presence of only a minor fraction of CH_2Si_2 units in SiCO, if at all, thus challenging theoretical predictions based on models obtained by replacing O by C in amorphous silica networks.[41–43]

EPR spectroscopy

The EPR spectra of the cross-linked PDCs are shown in Figure 6a. These spectra show a significant decrease in line width from 0.35 mT to 0.15 mT with increasing carbon content in the SiCO ceramics from 14% to 55% (Figure 6b). This observation can be explained by changes of the hyperfine interactions between the nuclear and electronic magnetic moment of hydrogen atoms bonded or adjacent to carbon. With the increase of the carbon content the density of dangling bonds and thus paramagnetic defects grows, which causes an increase of electron spin exchange interactions, which reduces the line width in the EPR spectra, as explained by Adronenko et al.[60] This finding is in good agreement with the Hahn-echo ^{13}C MAS NMR data (Figure 4b) discussed above. Cross-linking of the carbon-richer polymer precursors favors the formation of free carbon phases and leads to an increasing number of paramagnetic dangling bonds.

Conclusion

The structural composition of polymer-derived silicon oxycarbide ceramics (SiCO) containing different carbon contents (SiCO-C14%, SiCO-C24%, SiCO-C36% and SiCO-C55%) has been investigated by applying ^{13}C and ^{29}Si solid-state MAS NMR spectroscopy. The ^{29}Si MAS NMR spectra of SiCO ceramics show significant line broadening compared to the ^{29}Si MAS NMR spectra of the preceramic precursors (PMS-MK, SPR-212, SILRES-604 and RD-684), which indicates increased structural disorder in the PDC networks caused by cross-linking. From deconvolution of the ^{29}Si MAS NMR spectra, the formation of different SiC_xO_{4-x} structural units such as SiO_4, $SiCO_3$, SiC_2O_2, SiC_4 and

© 2023 The Authors. ChemSusChem published by Wiley-VCH GmbH

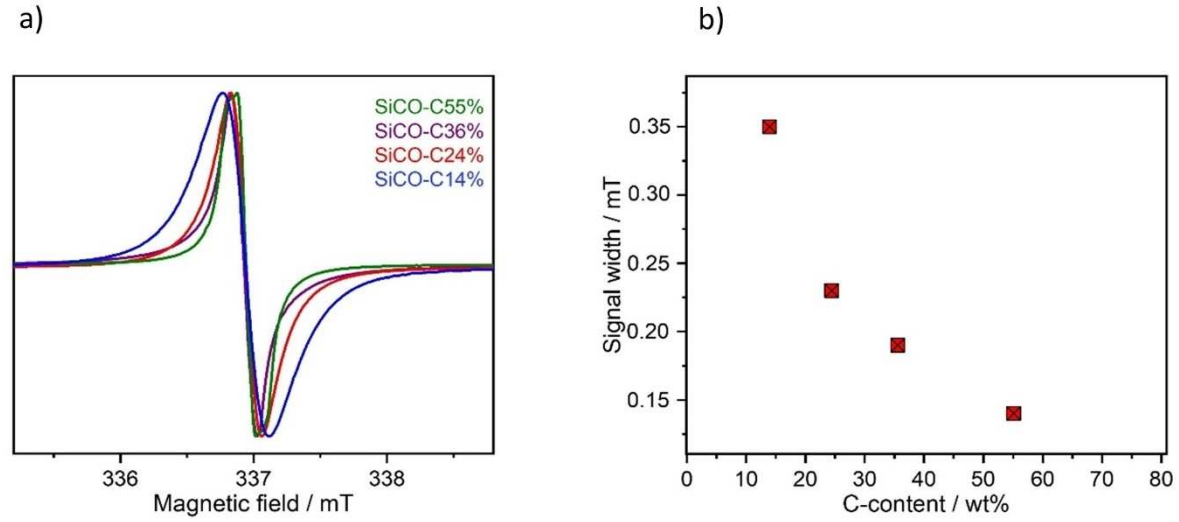

Figure 6. a) EPR spectra of the SiCO samples synthesized from preceramic polymers with different carbon content recorded at RT. Spectra are normalized on the peak maximum. Note: Although spectra were not centered, the center positions only vary by 0.02 mT, which is within the error margins. b) Signal widths in the EPR-spectra of the PDCs displayed as a function of the total carbon content calculated from the elementary analysis.

SiC_3O is identified. These chemical shifts are in good agreement with the calculated values at the DFT level of theory. The ^{13}C MAS NMR spectra indicate that the SiCO-PDCs contain sp^3 bonded carbon species such as CSi_4, SiC_xO_{4-x} as well as aliphatic carbons originating from the manufacturing process, sp^2 bonded graphene layers and C=O containing sites. This assignment of carbon structures has been exemplary proved by ^{1}H-^{13}C FSLG-HETCOR MAS NMR of SiCO-C14% at 14.1 T.

In the EPR spectra of the PDCs, the decrease in the line width with increasing carbon content indicates the formation of paramagnetic dangling bonds, when carbon-richer preceramic precursors are used for the cross-linking.

To summarize, the formation of carbon-free phases and paramagnetic defects strongly depends on the composition of the preceramic polymers. This basic work provides important local structural information on SiCO ceramics which are the basis to understand their electrochemical properties in energy storage devices based on alkali metal/ion such as Na/Na^+ in the near future.

Acknowledgements

Financial support by the European Union in the frame of the EU project SIMBA (Sodium-Ion and Sodium Metal Batteries for efficient and sustainable next-generation energy storage) under grant agreement number 963542 is gratefully acknowledged. Open Access funding enabled and organized by Projekt DEAL.

Conflict of Interest

There are no conflicts to declare.

Data Availability Statement

The data that support the findings of this study are available in the supplementary material of this article.

Keywords: Ceramics · defects · density functional calculations · EPR spectroscopy · NMR spectroscopy

[1] a) K. Feng, M. Li, W. Liu, A. G. Kashkooli, X. Xiao, M. Cai, Z. Chen, *Small* **2018**, *14*, 1702737; b) R. Bhandavat, Z. Pei, G. Singh, *Nanomater. Energy* **2012**, *1*, 324–337; c) D. Stampatori, P. P. Raimondi, M. Noussan, *Energies* **2020**, *13*, 2638.
[2] H. Fukui, H. Ohsuka, T. Hino, K. Kanamura, *ACS Appl. Mater. Interfaces* **2010**, *2*, 998–1008.
[3] M. Graczyk-Zajac, L. Toma, C. Fasel, R. Riedel, *Solid State Ionics* **2012**, *225*, 522–526.
[4] H. Fukui, H. Ohsuka, T. Hino, K. Kanamura, *J. Electrochem. Soc.* **2013**, *160*, A1276–A1281.
[5] a) M. S. Kolathodi, L. David, M. A. Abass, G. Singh, *RSC Adv.* **2016**, *6*, 74323–74331; b) S. Mukherjee, Z. Ren, G. Singh, *J. Phys. D* **2018**, *51*, 463001.
[6] C. Chandra, H. S. Cahyadi, S. Alvin, W. Devina, J.-H. Park, W. Chang, K. Y. Chung, S. K. Kwak, J. Kim, *Chem. Mater.* **2020**, *32*, 410–423.
[7] E. Šić, M. Melzi d'Eril, K. Schutjajew, M. J. Graczyk-Zajac, H. Breitzke, R. Riedel, M. Oschatz, T. Gutmann, G. Buntkowsky, *Batteries & Supercaps* **2022**, *5*, e20220006.
[8] M. A. Abass, A. A. Syed, C. Gervais, G. Singh, *RSC Adv.* **2017**, *7*, 21576–21584.
[9] a) L. David, K. M. Shareef, M. A. Abass, G. Singh, *RSC Adv.* **2016**, *6*, 53894–53902; b) L. David, R. Bhandavat, U. Barrera, G. Singh, *Nat. Commun.* **2016**, *7*, 10998; c) D. Ahn, R. Raj, *J. Power Sources* **2011**, *196*, 2179–2186.
[10] P. Colombo, G. Mera, R. Riedel, G. D. Sorarù, *J. Am. Ceram. Soc.* **2010**, *93*, 1805–1837.
[11] E. Barrios, L. Zhai, *Mol. Syst. Des. Eng.* **2020**, *5*, 1606–1641.
[12] a) A. Karakuscu, R. Guider, L. Pavesi, G. D. Soraru, *J. Am. Ceram. Soc.* **2009**, *92*, 2969–2974; b) A. B. Kousaalya, X. Zeng, M. Karakaya, T. Tritt, S. Pilla, A. M. Rao, *ACS Appl. Mater. Interfaces* **2018**, *10*, 2236–2241.
[13] a) F. Roth, C. Schmerbauch, E. Ionescu, N. Nicoloso, O. Guillon, R. Riedel, *J. Sens. Sens. Syst.* **2015**, *4*, 133–136; b) F. Roth, O. Guillon, E. Ionescu, N. Nicoloso, C. Schmerbauch, R. Riedel, *Piezoresistive Ceramics for High-Temperature Force and Pressure Sensing ITG-Fachbericht*, *250*, **2014**, VDE,

© 2023 The Authors. ChemSusChem published by Wiley-VCH GmbH

Berlin; c) E. Ricohermoso, F. Klug, H. Schlaak, R. Riedel, E. Ionescu, *Mater. Des.* **2022**, *213*, 110323; d) E. Ricohermoso, F. Rosenburg, F. Klug, N. Nicoloso, H. F. Schlaak, R. Riedel, E. Ionescu, *Open Ceram.* **2021**, *5*, 100057.
[14] a) A. Tamayo, M. A. Mazo, M. D. Veiga, R. Ruiz-Caro, F. Notario-Pérez, J. Rubio, *Mater. Sci. Eng. C* **2017**, *75*, 1097–1105; b) C. Vakifahmetoglu, D. Zeydanli, V. C. Ozalp, B. A. Borsa, G. D. Soraru, *Mater. Des.* **2018**, *140*, 37–44.
[15] a) Z. Ren, S. B. Mujib, G. Singh, *Materials* **2021**, *14*, 614; b) M. D. Nguyen, J. W. Bang, A. S. Bin, S.-R. Kim, Y. Kim, K. H. Hwang, V.-H. Pham, W.-T. Kwon, *J. Eur. Ceram. Soc.* **2017**, *37*, 2001–2010.
[16] a) A. Francis, *Mater. Res. Express* **2018**, *5*, 62003; b) Y. Song, L. He, X. Zhang, F. Liu, N. Tian, Y. Tang, J. Kong, *J. Phys. Chem. C* **2017**, *121*, 24774–24785.
[17] E. Ionescu, C. Linck, C. Fasel, M. Müller, H. Kleebe, R. Riedel, *J. Am. Ceram. Soc.* **2010**, *93*, 241–250.
[18] C. Stabler, E. Ionescu, M. Graczyk-Zajac, I. Gonzalo-Juan, R. Riedel, *J. Am. Ceram. Soc.* **2018**, *101*, 4817–4856.
[19] C. Liu, R. Pan, C. Hong, X. Zhang, W. Han, J. Han, S. Du, *J. Eur. Ceram. Soc.* **2016**, *36*, 395–402.
[20] G. D. Soraru, R. Campostrini, A. A. Ejigu, E. Zera, P. Jana, *J. Ceram. Soc. Jpn.* **2016**, *124*, 1023–1029.
[21] F. Rosenburg, B. Balke, N. Nicoloso, R. Riedel, E. Ionescu, *Molecules* **2020**, *25*, 5919.
[22] a) Q. Wen, F. Qu, Z. Yu, M. Graczyk-Zajac, X. Xiong, R. Riedel, *J. Adv. Ceram.* **2022**, *11*, 197–246; b) E. Bernardo, L. Fiocco, G. Parcianello, E. Storti, P. Colombo, *Materials* **2014**, *7*, 1927–1956.
[23] G. Mera, M. Gallei, S. Bernard, E. Ionescu, *Nanomaterials* **2015**, *5*, 468–540.
[24] R. Riedel, G. Mera, R. Hauser, A. Klonczynski, *J. Ceram. Soc. Jpn.* **2006**, *114*, 425–444.
[25] S. J. Widgeon, S. Sen, G. Mera, E. Ionescu, R. Riedel, A. Navrotsky, *Chem. Mater.* **2010**, *22*, 6221–6228.
[26] a) G. Mera, A. Navrotsky, S. Sen, H.-J. Kleebe, R. Riedel, *J. Mater. Chem. A* **2013**, *1*, 3826; b) F. Babonneau, G. D. Soraru, G. D'Andrea, S. Dire, L. Bois, *Mater. Res. Soc. Symp. Proc.* **1992**, *271*, 789–794; c) R. Kalfat, F. Babonneau, N. Gharbi, H. Zarrouk, *J. Mater. Chem.* **1996**, *6*, 1673–1678; d) G. Trimmel, R. Badheka, F. Babonneau, *J. Sol-Gel Sci. Technol.* **2003**, *23*, 279–283; e) M. Weinmann, E. Ionescu, R. Riedel, F. Aldinger in *Handbook of Advanced Ceramics*, Elsevier, **2013**; f) F. Rosenburg, E. Ionescu, N. Nicoloso, R. Riedel, *Materials* **2018**, *11*, 93; g) F. Roth, P. Waleska, C. Hess, E. Ionescu, N. Nicoloso, *J. Ceram. Soc. Jpn.* **2016**, *124*, 1042–1045; h) H.-J. Kleebe, C. Turquat, G. D. Sorarù, *J. Am. Ceram. Soc.* **2001**, *84*, 1073–1080.
[27] E. Ionescu, H.-J. Kleebe, R. Riedel, *Chem. Soc. Rev.* **2012**, *41*, 5032–5052.
[28] a) M. Idrees, S. Batool, Q. Zhuang, J. Kong, I. Seok, J. Zhang, H. Liu, V. Murugadoss, Q. Gao, Z. Guo, *Ceram. Int.* **2019**, *45*, 10572–10580; b) J. Kaspar, M. Graczyk-Zajac, S. Choudhury, R. Riedel, *Electrochim. Acta* **2016**, *216*, 196–202; c) Y. S. Kim, Y. L. Joo, Y.-J. Kwark, *J. Mater. Sci. Technol.* **2016**, *32*, 195–199; d) K. Kitada, O. Pecher, P. C. M. M. Magusin, M. F. Groh, R. S. Weatherup, C. P. Grey, *J. Am. Chem. Soc.* **2019**, *141*, 7014–7027; e) D. Knozowski, M. Graczyk-Zając, D. Vrankovic, G. Trykowski, M. Sawczak, D. M. de Carolis, M. Wilamowska-Zawłocka, *Composites Part B* **2021**, *225*, 109302; f) B. Krüner, C. Odenwald, N. Jäckel, A. Tolosa, G. Kickelbick, V. Presser, *ACS Appl. Energ. Mater.* **2018**, *1*, 2961–2970; g) N. Liao, M. Zhang, B. Zheng, W. Xue, *Appl. Mater. Today* **2020**, *18*, 100434; h) P. Stein, D. Vrankovic, M. Graczyk-Zajac, R. Riedel, B.-X. Xu, *JOM* **2017**, *69*, 1524–1531; i) P. Vallachira Warriam Sasikumar, E. Zera, M. Graczyk-Zajac, R. Riedel, G. D. Soraru, *J. Am. Ceram. Soc.* **2016**, *99*, 2977–2983.
[29] a) W. Bai, S. Widgeon, S. Sen, *J. Non-Cryst. Solids* **2014**, *386*, 29–33; b) W. Szczypka, A. Koleżyński, *J. Mol. Struct.* **2020**, *1208*, 127930; c) R. Sujith, S. Jothi, A. Zimmermann, F. Aldinger, R. Kumar, *Int. Mater. Rev.* **2021**, *66*, 426–449; d) N. Yang, K. Lu, *J. Am. Ceram. Soc.* **2021**, *104*, 5379–5391.
[30] P. Dibandjo, M. Graczyk-Zajac, R. Riedel, V. S. Pradeep, G. D. Soraru, *J. Eur. Ceram. Soc.* **2012**, *32*, 2495–2503.
[31] a) C. Chandra, J. Kim, *Chem. Eng. J.* **2018**, *338*, 126–136; b) M. Weinberger, C. Pfeifer, S. Schindler, T. Diemant, R. J. Behm, M. Wohlfahrt-Mehrens, *J. Mater. Chem. A* **2015**, *3*, 23707–23715; c) J. Kaspar, M. Storch, C. Schitco, R. Riedel, M. Graczyk-Zajac, *J. Electrochem. Soc.* **2016**, *163*, A156–A162.
[32] C. Stabler, A. Reitz, P. Stein, B. Albert, R. Riedel, E. Ionescu, *Materials* **2018**, *11*, 279.
[33] I. Scholz, P. Hodgkinson, B. H. Meier, M. Ernst, *J. Chem. Phys.* **2009**, *130*, 114510.
[34] B. Kumari, M. Brodrecht, T. Gutmann, H. Breitzke, G. Buntkowsky, *Appl. Magn. Reson.* **2019**, *50*, 1399–1407.
[35] J. Enkovaara et al., *J. Phys. Condens. Matter* **2010**, *22*, 253202.
[36] A. Hjorth Larsen et al., *J. Phys. Condens. Matter* **2017**, *29*, 273002.
[37] G. Kresse, J. Furthmüller, *Phys. Rev. B* **1996**, *54*, 11169–11186.
[38] P. E. Blöchl, *Phys. Rev. B* **1994**, *50*, 17953–17979.
[39] J. P. Perdew, K. Burke, M. Ernzerhof, *Phys. Rev. Lett.* **1996**, *77*, 3865–3868.
[40] H. J. Monkhorst, J. D. Pack, *Phys. Rev. B* **1976**, *13*, 5188–5192.
[41] N. Liao, B. Zheng, H. Zhou, W. Xue, *J. Mater. Chem. A* **2015**, *3*, 5067–5071.
[42] H. Ding, M. J. Demkowicz, *Sci. Rep.* **2015**, *5*, 13051.
[43] H. Sun, K. Zhao, *ACS Appl. Mater. Interfaces* **2017**, *9*, 35001–35009.
[44] a) P. Kroll, *J. Mater. Chem.* **2003**, *13*, 1657; b) P. Kroll, *J. Mater. Chem.* **2010**, *20*, 10528; c) I. Ponomarev, A. C. T. van Duin, P. Kroll, *J. Phys. Chem. C* **2019**, *123*, 16804–16812.
[45] J. P. Nimmo, P. Kroll, *J. Phys. Chem. C* **2014**, *118*, 29952–29961.
[46] A. P. Thompson et al., *Comput. Phys. Commun.* **2022**, *271*, 108171.
[47] P. Erhart, K. Albe, *Phys. Rev. B* **2005**, *71*, 35211.
[48] L. C. Erhard, J. Rohrer, K. Albe, V. L. Deringer, *npj Comput. Mater.* **2022**, *8*, 90.
[49] a) K. Chen, *Int. J. Mol. Sci.* **2020**, *21*, 5666; b) S. Leonardelli, L. Facchini, C. Fretigny, P. Tougne, A. P. Legrand, *J. Am. Ceram. Soc.* **1992**, *114*, 6412–4618.
[50] M. Luhmer, J. B. d'Espinose, H. Hommel, A. P. Legrand, *Magn. Reson. Imaging* **1996**, *14*, 911–913.
[51] R. J.-C. Dubey, P. V. W. Sasikumar, N. Cerboni, M. Aebli, F. Krumeich, G. Blugan, K. V. Kravchyk, T. Graule, M. V. Kovalenko, *Nanoscale* **2020**, *12*, 13540–13547.
[52] I. Hung, E. Ionescu, J. Sen, Z. Gan, S. Sen, *J. Phys. Chem. C* **2021**, *125*, 4777–4784.
[53] I. G. Shenderovich, D. Mauder, D. Akcakayiran, G. Buntkowsky, H.-H. Limbach, G. H. Findenegg, *J. Phys. Chem. B* **2007**, *111*, 12088–12096.
[54] W. Fortuniak, J. Chojnowski, S. Slomkowski, A. Nyczyk-Malinowska, P. Pospiech, U. Mizerska, *Mater. Chem. Phys.* **2015**, *155*, 83–91.
[55] Q. D. Nghiem, A. Asthana, I.-K. Sung, D.-P. Kim, *J. Mater. Res.* **2006**, *21*, 1543–1549.
[56] P. Dibandjo, S. Diré, F. Babonneau, G. D. Soraru, *J. Non-Cryst. Solids* **2010**, *356*, 132–140.
[57] C. Sugie, A. Navrotsky, S. Lauterbach, H.-J. Kleebe, G. Mera, *Materials* **2021**, *14*, 4075.
[58] V. Klimavicius, H. Hilbig, T. Gutmann, G. Buntkowsky, *J. Phys. Chem. C* **2021**, *125*, 7321–7328.
[59] a) J. D. Satterlee, *Concepts Magn. Reson. Part A* **1990**, *2*, 119–129; b) M. J. Knight, I. C. Felli, R. Pierattelli, L. Emsley, G. Pintacuda, *Acc. Chem. Res.* **2013**, *46*, 2108–2116.
[60] S. I. Andronenko, I. Stiharu, S. K. Misra, *J. Appl. Phys.* **2006**, *99*, 113907.

Revised manuscript received: March 8, 2023
Accepted manuscript online: March 9, 2023
Version of record online: April 18, 2023

© 2023 The Authors. ChemSusChem published by Wiley-VCH GmbH